Composites Science and Technology 91 (2014) 71–81

Contents lists available at ScienceDirect

Composites Science and Technology

journal homepage: www.elsevier.com/locate/compscitech

Fatigue of multiscale composites with secondary nanoplatelet reinforcement: 3D computational analysis

Gaoming Dai *, Leon Mishnaevsky Jr. *

Department of Wind Energy, Technical University of Denmark, Risø Campus, Frederiksborgvej 399, DK-4000 Roskilde, Denmark

ARTICLE INFO

Article history:
Received 9 October 2013
Received in revised form 20 November 2013
Accepted 24 November 2013
Available online 8 December 2013

Keywords:
A. Nanocomposites
A. Polymer–matrix composites (PMCs)
B. Fatigue
C. Computational mechanics
C. Finite element analysis (FEA)

ABSTRACT

3D numerical simulations of fatigue damage of multiscale fiber reinforced polymer composites with secondary nanoclay reinforcement are carried out. Macro–micro FE models of the multiscale composites are generated automatically using Python based software. The effect of the nanoclay reinforcement (localized in the fiber/matrix interface (fiber sizing) and distributed throughout the matrix) on the crack path, damage mechanisms and fatigue behavior is investigated in numerical experiments. It was observed that the composites with secondary nanoreinforcement localized in the fiber sizing ensure higher lifetime and damage resistance than those with nanoreinforcement dispersed throughout the matrix. Crack bridging by nanoparticles was observed mainly in composites with randomly oriented nanoplatelets and clusters, while the crack path deviation was strongest in the composites with aligned nanoplatelets. Multiscale composites with exfoliated nanoreinforcement and aligned nanoplatelets ensure the better fatigue resistance than those with intercalated/clustered and randomly oriented nanoreinforcement.

1. Introduction

The development of composites with hierarchical structures represents a promising reserve of the enhancement of service properties of composites [1,2]. Composite materials with hierarchical structures make it possible to combine the advantages of microscale reinforcement of composites with those of nanoreinforcement.

Since it is known that properties of polymer can be drastically enhanced by adding a few weight percents of nanoreinforcement [3], it can be also expected that comparable positive effects can be achieved by nanomodification of fiber reinforced polymer composites. The addition of nanoreinforcement to the polymer matrix can lead to the improvement in the elastic modulus and strength (clearly observed in rubbery epoxy and polyamide with exfoliated nanoclay (NC); less clear in glassy epoxy), as well reduced ductility and constrained plastic deformation [4,5]. However, the transfer of these effects on fiber reinforced composites is not always apparent: some properties of the composites are controlled by fiber properties, some by matrices and some by their interaction; further, the matrix is in much more complex stress state in the composite.

Here, we consider the composites with epoxy matrix, reinforced by glass fibers and nanoclays at nanolevel, and seek to analyze the effect of nanoclay reinforcement of the fatigue properties of these materials, widely used among other for wind turbine blades. As for now, this combination of constituents is less expensive as compared with carbon and carbon nanotube (CNT) reinforcement and/or thermoset matrices, thus, allowing more broad potential use of the multiscale materials.

The effects of small additions of nanoreinforcement in fiber reinforced polymers on the mechanical properties and strength of materials have been investigated in a number of works [6–13]. The mechanical properties and strength improvement due to the nanoclay addition was observed in numerous studies: e.g., increase of tensile strength, strain and tensile modulus to failure (~20%, 13% and 60%, respectively, at wt% 5%). The increase of fatigue life up to 74% with 3 wt% clay content (NC/carbon fibers/epoxy TT fatigue, [8]), 53% and 85% increase of mode I interlaminar FT by with 2 and 4 phr NC respectively, (NC/carbon fiber/epoxy [9]), 26% increase of flexural modulus 26% at 3 wt%, 30% increase of quasi-static FT increases by 60% at 3 wt% (peak value). (NC/carbon fibers/epoxy [4]), 4–5 times increased fatigue life under WISPERX loading (glass fiber/hybrid particles/epoxy [10]), UTS, Young's modulus, flexural strength, ILSS and microhardness increase up to 5 wt% of NC (by 30%, 38%, 120%, 25%, 70% and 25% respectively) and decrease after that (NC/glass/epoxy [11]), 21–30% improvement on the interfacial shear strength at 2–14 vol.% silica (epoxy/carbon fiber/silica nanoparticles under single fiber fragmentation [14]). In these studies, it was also observed that the secondary nanoclay reinforcement changes the damage and fracture mechanisms of composites: narrower dimples on fracture surfaces and more dimples of smaller sizes, more damage at early cycles (crack initiation

* Corresponding authors. Tel.: +45 60697858; fax: +45 4677 5758.
E-mail addresses: ggda@dtu.dk (G. Dai), lemi@dtu.dk (L. Mishnaevsky Jr.).

0266-3538/$ - see front matter © 2013 Elsevier Ltd. All rights reserved.
http://dx.doi.org/10.1016/j.compscitech.2013.11.024

stage) (due to cleavage of tactoids and intergallery debonding), but less damage later (nanocrack coalescence and propagation). NC leads to crack deflection, fiber/matrix bonding is improved by the fracture surface becomes rougher and textured [8], crack propagates around NC agglomerates and makes longer path, with pining and path bifurcations (river markings near agglomerates) [4], matrix cracking is suppressed and the delamination delayed [10], nanoclay improves notch resistance of epoxy; with agglomeration and clustering, NC becomes site for damage initiation; high aspect ratio of the nano-additive constrains the micro-cracks growth and delays failure [12]. One can see that the results on the effect of secondary nanoreinforcement on the service properties of composites and damage mechanisms are inconsistent and strongly depend on the conditions of experiment, used technologies of the material production and chosen constituents. Still, the nanoclay reinforcements seem to have a high potential for the material enhancement.

Some hints on the damage and toughening mechanisms in fiber reinforced composites (FRC) with secondary nanoclay (NC) reinforcement can be also obtained from the analysis of composites with secondary carbon nanotube (CNT) reinforcement. Díez-Pascual et al. [15] reviewed literature on failure mechanisms in hierarchical CNT-modified fiber-reinforced thermoplastic composites, and concluded that matrix-dominated properties such as flexural and interlaminar shear strength are drastically improved by the CNT additions, while fiber-controlled properties (such as tensile strength and stiffness) are improved only slightly. In [16–18], the effect of morphology and distribution of CNTs on the damage and fracture and composites was studied. The authors compared the composites with CNTs dispersed in matrix and distributed in fiber sizings. The CNT crack initiation toughness increases (by 10% if CNTs in sizing and by 25% if in matrix) and the crack propagation toughness decreases (by 30–50%) when CNTs are placed in sizing [17]. However, in the system with carbon fibers, both crack initiation and propagation energies were improved by CNT addition in matrix [18,19], what is related with CNT bridging and other toughening mechanisms (crack deflection, blocking). In [20], it was shown that the tensile strength of glass fibers increases significantly with increasing CNT content up to a certain level, depending on the type of CNTs. As said, the transferability of the observations of CNT toughening and strengthening mechanisms on nanoclay reinforcement is questionable; still, it can give us some hints on the mechanisms of interaction of micro- and nanoreinforcement in composites.

In this paper, we seek to study the effect of distribution and arrangement of the secondary nanoreinforcement on the fatigue resistance of multiscale composites, using numerical experiments [2,5,21–23]. We consider here the multiscale glass fiber reinforced epoxy composites with nanoclay reinforcement in the matrix or in the fiber sizing subject to cyclic compression-compression loading. As a result of these studies, we seek to develop recommendations toward improvement of the composite performances by using nanoclay secondary reinforcement.

2. 3D multiscale computational model of multiscale composites

2.1. Macro–micro multiple-step modeling

The structures of multiscale composites with primary fiber and secondary nanoparticle/nanoclay reinforcements are characterized by the large scale difference of structural elements (Fig. 1). Under such conditions, it is hardly practicable to simulate both scale levels in framework of one and the same micromechanical model [24–26]. Rather, we employ the concept of macro–micro multiple-step modeling strategy to analyze the multiscale materials with different dimensional scales. In our model, we divide the structure into two levels.

The macro (upper level) unit cell contains three phases: the matrix, fibers and interface layers between them (following the "third layer" model of interfaces from [27–29]; this third layer includes fiber sizing, interphases, fiber surface roughness and allow to simulate the interface damage as a 3D process). Both matrix and the interface layer might contain nanoreinforcement (see Fig. 2).

The microscale (lower level) unit cell includes the nanoplatelets reinforcement (exfoliated nanoplatelets and intercalated nanoplatelets/cluster) in matrix and/or interfaces, polymer matrix as well as the "nano-interface layer" (areas of polymer modified due to the interaction and bonding with nanoscale platelets and polymer chain constraints, with properties which are different from those of neat polymer) and the "intra-stack phase" (see [2,5,30]). As noticed in [2,30], the properties of the polymer matrix between nanoplatelets in a cluster are different from both the pure matrix and the "nano-interface layer" around (not between) the nanoplatelets. That is why we, following [2], consider one more phase at the microlevel, namely "intra-stack interface layer phase".

The simulation method used in this paper includes two steps: At the first step, the global analysis is carried out. The macro-level structure is simulated with rough FE meshing and stress and displacement distributions at the macroscale are obtained. The macroscale model was subject to cyclic compressive–compressive loading. After some loading, one of the fibers in the model failed (in all the models). After the first crack is formed in a fiber, a submodel unit cell is placed in the matrix or in the interface layer near the tip of the crack formed in the fiber, or in the matrix, also near the crack tip of the fiber crack. A submodel, which is part of the global model, is built, with fine mesh. The boundary conditions (the stress and displacement distribution obtained from the global analysis) are transferred to the submodel, and then repeated cyclically. Then, the crack growth in the submodel is simulated using extended finite element method (XFEM). This damage mechanism was also reported by Karippal et al. [11], who noticed that the fiber breaking is dominant failure mode in glass/epoxy/nanoclay composites.

2.2. Macro- and micromodels design

Both macro- and microscale unit cells were generated using the special Python based software code for the automatic generation of 3D multi-element unit cell FE models of hybrid composites [2,27,28]. The program allows varying the cylindrical reinforcing element (fiber or platelet) orientation (random, aligned, and aligned at some angle to the loading direction), radii, and arrangements of the fibers. All the reinforcing elements are randomly arranged in the matrix [22]. The coordinates of the points are generated using the Mersenne Twister random number generator. Each fiber or platelet is associated with a misalignment angle, which is also generated using the random number generator.

The macro-model analysis saves the time-dependent values of variables (i.e. stress and displacement field) of the "seed nodes" which located on the boundary between macro model and micro model after the macro-level analysis. The micro-model inherits these data as the initial boundary condition and together with other added boundary condition (if needed) to go on the analysis.

The macro-level unit cell model have dimensions of 80 μm × 80 μm × 80 μm, with 15 glass fibers and fraction of fibers 47.1%. The matrix–fiber interfaces layers had a thickness of 0.62 μm [27–29].

The submodels, located in the interface layers, have the dimensions of 0.62 μm × 0.62 μm × 0.47 μm and the same number of nanoplatelets.

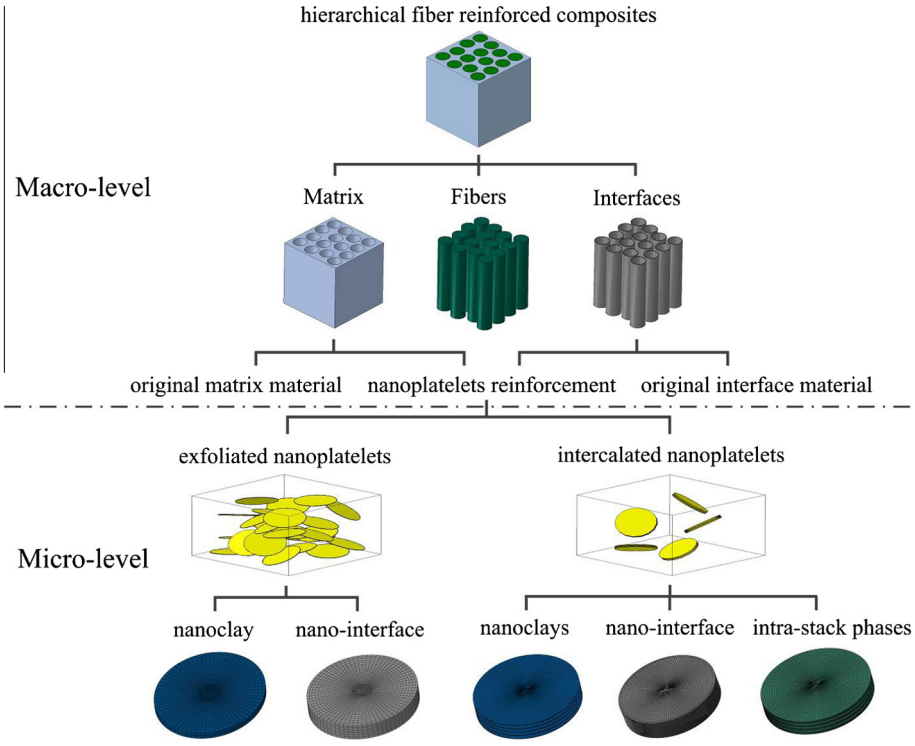

Fig. 1. Illustration of structure of hierarchical fiber reinforced composite with nanoplatelets reinforcement.

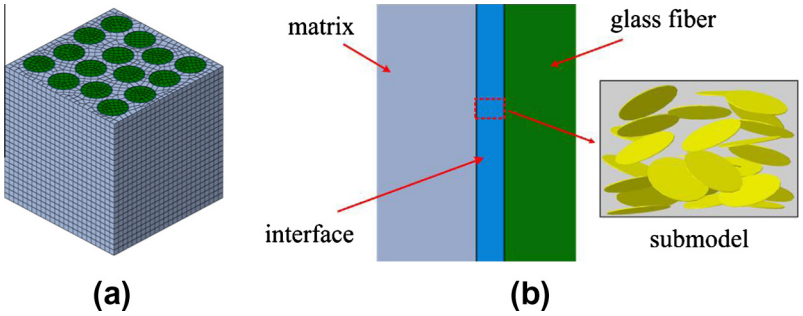

Fig. 2. Macroscale finite element model (a) and the schema of submodel–macromodel (b).

In order to compare the cases of nanoplatelets located in fiber sizing (fiber/matrix interface layer) and in the matrix, we should consider unit cells with equal volume content of nanoclay material and amount of nanoplatelets. Taking the volume fraction of nanoplatelets in the interface layer 0.48%, one can calculate the volume of all the nanoplatelet materials in all the interface layers of the macromodel as:

$$V_{ti} = n_G \pi (R_i^2 - R^2) H = 3.88 \times 10^4 \ \mu\text{m}^3 \tag{1.1}$$

where n_g – the number of fibers, R – fiber radius, R_i – fiber radius plus the interface layer thickness, H – height of the model. The volume content of a single nanoplatelet is:

$$V_{sn} = \pi r^2 t = 3.14 \times 10^{-5} \ \mu\text{m}^3 \tag{1.2}$$

The total number of nanoplatelets in the macromodel is:

$$n_{\text{nanoplatelet}} = \frac{0.0048 V_{ti}}{V_{sn}} = 5.93 \times 10^6 \tag{1.3}$$

Here t – thickness of the nanoplatelet. Then, the volume fraction of nanoplatelets in the matrix can be calculated as (since the number and the fraction of nanoplatelets should be the same in both cases):

$$V_{Mf} = \frac{n_{\text{nanoplatelet}} V_{sn}}{V_M} \tag{1.4}$$

Here, V_M stands for the volume content of matrix, which can be described as:

$$V_M = V_T - V_G - V_{ti} \tag{1.5}$$

in which V_T is the total volume of the unit cell, V_G is the volume content of all the glass fibers:

$$V_T = \text{LWH} = 5.12 \times 10^5 \ \mu\ \text{m}^3$$
$$V_G = n_G \pi R^2 H = 2.41 \times 10^5 \ \mu\text{m}^3$$

Substituting Eqs. (1.1 and 1.6) into Eq. (1.5), we have

$$V_M = 2.322 \times 10^5 \ \mu\text{m}^3 \tag{1.7}$$

Then, the volume fraction of nanoplatelet in the matrix can be calculated as:

$$V_{fM} = \frac{n_{\text{nanoplatelet}} V_{sn}}{V_M} \times 100\% = 0.08\% \tag{1.8}$$

Apparently, the micro-level unit cell for the matrix which contains the same amount of nanoplatelets should be 6 times larger (in volume) than the unit cell for the interface layer with the same

amount of nanoplatelets (i.e., 1.81 times larger in each dimension). Thus, the sub-models located in the matrix, had the dimensions 1.13 μm × 1.13 μm × 0.85 μm.

2.3. Numerical implementation of fatigue analysis

First, we introduced initial defects into the macroscale model by subjecting the unit cell to a quasi-static load before the cyclic loading. As the criterion of the initial defect formation, we used the maximum principal stress criterion. After the initial defects (with the sizes of the order of 1–2 finite elements) are formed, the fatigue modeling procedure for macroscale model is run. Both the crack growth onset and crack propagation are described using the Paris law. The criterion for the onset of fatigue crack (crack starting growth at the crack tip under the fatigue loading) can be described as $\frac{N_O}{c_1(\Delta G)^{c_2}} \geqslant 1$, where N_O stands for the number of cycles to the onset, c_1 and c_2 are material constants while ΔG represents the range of strain energy release rate, for example, the difference between the strain energy release rate at the peak and valley loading. When this equation is satisfied and, at the same time, $G_{\max}$ obeys the condition that $G_{th} < G_{\max} < G_c$, the static procedure generated "initial defect" will be stimulated and starting growth. Here, G_{th}, G_c and $G_{\max}$ mean the threshold value of strain energy release rate, critical strain energy release rate and strain energy release rate corresponding to the maximum loaded of the structure, respectively.

The fatigue crack growth was characterized by 4 material constants: c_1, c_2, c_3 and c_4 where the last two enter the fatigue crack growth rate as a power law: $\frac{da}{dN} = c_3(\Delta G)^{c_4}$, where da/dN is the crack growth rate (fatigue crack length growth per loading cycle).

The crack propagation analysis is carried out in the framework of the linear elastic fracture mechanics (LEFM) approach and is based on the extended-FEM method [29,31]. The Virtual Crack Closure Technique (VCCT) [32,33] is employed to calculate the strain energy release rate at the crack tip.

2.4. Material properties, and boundary and loading conditions

The material properties of phases are listed in Table 1 [2,5,23,30]. The radius of nanoplatelets was taken 100 nm; the thickness was 1 nm in. The radius of nano-interface phase is 101 nm and the thickness is 1 nm. The intra-stack phase has the same radius as the nanoplatelet and a 3 nm thickness. The glass fiber has a radius of 8 μm and the matrix–fiber interface has the thickness of 0.62 μm [21]. The matrix' tensile strength was 68 MPa and compression strength 88 MPa. The tensile and compressive strengths of glass fiber are 2500 MPa and 1500 MPa, respectively. The matrix–fiber interface has tensile strength of 82 MPa and compression strength of 114 MPa, respectively. The tensile strength and compression strength of the intra-stack phase in nanoplatelet cluster is 40 MPa and 63 MPa, respectively. The tensile strength and compression strength of the nano-interface phase in nanoplatelet cluster is 53 MPa and 71 MPa, respectively.

The threshold and critical strain energy release rates of different material phases and different fracture modes are given as [34–38]: for the matrix: $G_{Ith} = 0.06$ kJ/m^2, $G_{IC} = 0.173$ kJ/m^2, $G_{IIth} = 0.24$ kJ/m^2, $G_{IIC} = 0.648$ kJ/m^2, $G_{IIIth} = 0.306$ kJ/m^2, $G_{IIIC} = 0.850$ kJ/m^2. For the glass fibers: $G_{Ith} = 0.21$ kJ/m^2, $G_{IC} = 0.682$ kJ/m^2, $G_{IIth} = 0.651$ kJ/m^2, $G_{IIC} = 2.245$ kJ/m^2, $G_{IIIth} = 0.994$ kJ/m^2, $G_{IIIC} = 2.923$ kJ/m^2. For the glass/fiber interface: $G_{Ith} = 0.18$ kJ/m^2, $G_{IC} = 0.461$ kJ/m^2, $G_{IIth} = 0.738$ kJ/m^2, $G_{IIC} = 2.05$ kJ/m^2, $G_{IIIth} = 0.893$ kJ/m^2, $G_{IIIC} = 2.35$ kJ/m^2. For the intra-stack phase in nanoplatelet cluster: $G_{Ith} = 0.168$ kJ/m^2, $G_{IC} = 0.421$ kJ/m^2, $G_{IIth} = 0.538$ kJ/m^2, $G_{IIC} = 1.85$ kJ/m^2, $G_{IIIth} = 0.813$ kJ/m^2, $G_{IIIC} = 2.13$ kJ/m^2. For the nano-interface layer phase: $G_{Ith} = 0.176$ kJ/m^2, $G_{IC} = 0.447$ kJ/m^2, $G_{IIth} = 0.652$ kJ/m^2, $G_{IIC} = 1.93$ kJ/m^2, $G_{IIIth} = 0.845$ kJ/m^2, $G_{IIIC} = 2.26$ kJ/m^2.

The four material constant parameters c_1, c_2, c_3 and c_4, which are used in the fatigue analysis, are defined based on works of other researchers [39–44]: for matrix: $c_1 = 2.8461 \times 10^{-9}$, $c_2 = -12.415$, $c_3 = 2.44 \times 10^6$ and $c_4 = 10.61$. For glass fiber: $c_1 = 3.74 \times 10^{-5}$, $c_2 = -6.415$, $c_3 = 7.89 \times 10^{-7}$ and $c_4 = 2.33$. For matrix–fiber interface: $c_1 = 5.7623 \times 10^{-7}$, $c_2 = -9.542$, $c_3 = 4.89 \times 10^{-8}$ and $c_4 = 11.153$. For intra-stack phase: $c_1 = 3.863 \times 10^{-6}$, $c_2 = -7.852$, $c_3 = 3.62 \times 10^{-9}$ and $c_4 = 12.243$. For nano-interface phase: $c_1 = 4.253 \times 10^{-6}$, $c_2 = -8.121$, $c_3 = 5.78 \times 10^{-8}$ and $c_4 = 11.743$.

The 3D model was subjected to the uniaxial periodic cyclic compressive loading (displacement) u along the Z-axis direction (the same values but opposite directions on both upper and lower faces of the box). All the simulations were carried out using ABAQUS/STANDARD finite element program (version 6.11). The three-dimensional 8-node linear brick finite element with reduced integration element C3D8R were used in the global scale analysis, and three-dimensional 4-node linear tetrahedron element C3D4 were used in the submodel analysis.

3. Effect of nanoreinforcement distribution on the crack morphology: 3D computational experiments

In this section, we carry out numerical simulations of the fatigue damage evolution of multiscale fiber + nanoclay reinforced composites under cyclic compression–compression loading. Various cases of distributions of secondary nanoreinforcement in the composites are considered, among them, nanoplatelets located in matrix–fiber interfaces (fiber sizing) and nanoplatelets in matrix, various alignment (aligned or random) and clustering degrees (intercalated or exfoliated nanoplatelet distributions). In the simulations, we seek to analyze how these different distributions influence the fatigue resistance of the multiscale composite.

3.1. Nanoplatelets reinforcement in interface of fiber reinforced composites

First, we study the effect of the nanoclay reinforcement distributed in the fiber/matrix interface layer on the fatigue behavior of the multiscale composites. We consider the aligned exfoliated nanoplatelets reinforcement, aligned intercalated nanoplatelets reinforcement, randomly oriented exfoliated nanoplatelets and randomly oriented intercalated nanoplatelets reinforcement in the matrix–fiber interfaces.

Let us compare the crack path in the different simulated subcells.

3.1.1. Aligned exfoliated nanoplatelets reinforcement in interface

Fig. 3a (left) gives the top view and lateral view of the microlevel unit cell with aligned exfoliated nanoplatelets. The model con-

Table 1
Material properties for different phase of nanocomposites.

	Matrix	Glass fiber	Matrix–fiber interface	Nanoplatelet	Nano-interface phase	Intra-stack phase
Young's modulus (GPa)	2.05	72	15	176	3.5	0.3
Shear modulus (GPa)	0.76	30	4.8	70	1.3	0.11
Poisson ratio	0.35	0.26	0.32	0.25	0.4	0.4

tains 25 exfoliated nanoplatelets. All the nanoplatelets are distributed randomly in unit cell volume but aligned perpendicular to the vertical axis.

Fig. 3a (right) shows the crack in the subcell under compression–compression cyclic loading. The direction of the crack propagation is from right to left. The right side of the model borders the fiber (first damaged) and the left side of the model borders the nanoreinforcement-free polymer matrix. Micro damage mechanisms such as the crack deflection, crack pinning (blocking) and the interface–nanoplatelet debonding are observed in the simulations. It is observed that micro-cracks generally initiate in the nano-interface phase of nanoplatelets, and then grow up and join together to form the main crack. The most typical mechanism observed is when a growing crack reaches a nanoplatelet and changes its direction (crack pinning or blocking). In the simulated crack path, totally 11 nanoplatelets were included into the crack path. The crack touched 7 nanoplatelets, changing direction. The debonding was observed on 6 nanoplatelets.

3.1.2. Aligned intercalated nanoplatelets reinforcement in interface

The submodel unit cell of a composite region in the fiber sizing with clustered, horizontal aligned platelets (clusters/intercalated structure) is shown in Fig. 3b (left)a (top and side views). The model contains 5 clusters, with 5 nanoplatelets in each cluster. The clusters are distributed randomly in the unit cell volume, and aligned perpendicularly to the vertical axis.

Fig. 3b (right) shows the fatigue crack in the unit cell with aligned intercalated nanoplatelets in the fiber sizing (interface). The crack starts from the right side of the model and ends in the left side of the model.

Large crack deflections are observed as well as the crack pinning and debonding. It is of interest that on the right side cluster, the crack pinning (happened when the crack meets the cluster upper surface) and debonding take place on the same cluster. Meanwhile, a micro-crack in the left-side cluster was first formed in the intra-stack phase (interface phase between nanoplatelets) (as observed in the simulations in [2,30]). It then penetrated the cluster, via the nano-interface phase surrounding the cluster. When the crack met with the other one, the large crack was formed.

One can see that the large crack went through two clusters. In the crack path, an area of crack growth between nanoplatelets in the cluster (nanoplatelet–nanoplatelet debonding), an area of crack growth through the nano-interface phase surrounding a cluster, and a crack pinning (i.e., crack changing direction reaching a nanoplatelet) were observed. A similar mechanism was also observed in by Quaresimin and Varley [12], who reported that with agglomeration and clustering, nanoclay platelets become site for damage initiation.

3.1.3. Random exfoliated nanoplatelets reinforcement in the interface layer

Fig. 3c (left) shows the microscale unit cell with random exfoliated nanoplatelets in the finer/matrix interface layer. The model includes 25 randomly distributed and randomly oriented nanoplatelets. The angles between the horizontal plane and the nanoplatelet plane were varied randomly, in the range 5–50°, using the random number generator.

The crack morphology is given in Fig. 3c (right). In the crack path, the crack bridged by nanoclay, as well as the crack pinning, interface debonding, and crack deflection were observed. (One should note that no crack bridging was seen in the previous two numerical experiments. Apparently, this occurs only in the case of randomly oriented, but not aligned nanoplatelets).

It is of interest that the crack path deviation from the horizontal line is lower in this case than in the case shown in Fig. 3a. One can assume that the aligned particle cause the stronger toughening effect via the crack path deviation than the randomly oriented particles. On the other side, the randomly oriented particles cause more crack bridging by nanoparticles. The crack path went via 9 nanoplatelets. In 4 places, the crack bridging was observed, and in 3 places, the crack pinning and debonding.

3.1.4. Random intercalated nanoplatelets reinforcement in interface layer

Fig. 3d (left) shows the microscale unit cell with random exfoliated nanoplatelets in the fiber/matrix interface. The model includes 5 randomly arranged and randomly aligned clusters. The angle varied in the range 5–50°. Fig. 3d (right) shows the fatigue crack in the unit cell with the aligned intercalated nanoplatelets. Two clusters in the middle of the model are involved in the final crack. The growth direction of the main crack is from right to left. Two typical damage mechanism, the intra-stack phase debonding and the crack bridging, take place in the right-side cluster and left-side cluster, respectively.

Also, the crack path deviation due to the nanoplatelets clusters was observed by Siddiqui et al. [4] in fiber composites with epoxy matrix and nanoclay reinforcement. The authors reported that cracks propagate around nanoclay agglomerates and make longer path, with pining and path bifurcations (river markings near agglomerates).

3.2. Nanoplatelets reinforcement in matrix of fiber reinforced composites

In this section, we consider the multiscale fiber reinforced composites with secondary nanoplatelet reinforcement distributed in the polymer matrix. The question is how the effect of secondary nanoreinforcement in matrix differs from the effect of the secondary reinforcement localized in the fiber sizing (considered in the Section 3.1). Apparently, the technologies of introduction of the nanoreinforcement in matrix and in fiber sizing are different; here, we seek the compare the effects of the nanoplatelet reinforcement keeping all the other factors constant except the geometrical ones.

In all the submodels, the same number of nanoplatelets is distributed as in the submodels placed in the interface layer from Section 3.1. This means that the volume fraction of nanoclay in the submodels located in the matrix models is much lower than that in the submodels located in the interface layers.

3.2.1. Aligned exfoliated nanoplatelets reinforcement distributed in the polymer matrix

A unit cell model of a matrix volume with horizontally aligned nanoplatelets is given in Fig. 4a (left) (top and side views). As already discussed in Section 2.2, the density of nanoplatelets in this model is much lower than those in the case of one in interface (Fig. 3a).

Fig. 4a (right) shows the crack path. The matrix-nanoplatelets debonding and crack pinning were observed in this case as well as the crack bridging. The crack went over 7 nanoplatelets. 5 sites debonding and 4 places of crack pinning were observed.

3.2.2. Aligned intercalated nanoplatelet reinforcement in matrix

Fig. 4b (left) shows the unit cell model with aligned intercalated nanoplatelets reinforcement. Each cluster contains 5 nanoplatelets, surrounded by a layer of nano-interface phase outside the whole cluster and the intra-stack phase between nanoplatelets. All the clusters are arranged perpendicularly to the vertical direction but randomly distributed in X and Y directions.

Fig. 4b (right) shows the crack path. The crack goes through two clusters, with the nanoplatelet–nanoplatelet debonding in the clusters as the main damage initiation mechanism. Micro-cracks are formed firstly in the intra-stack phase of clusters and con-

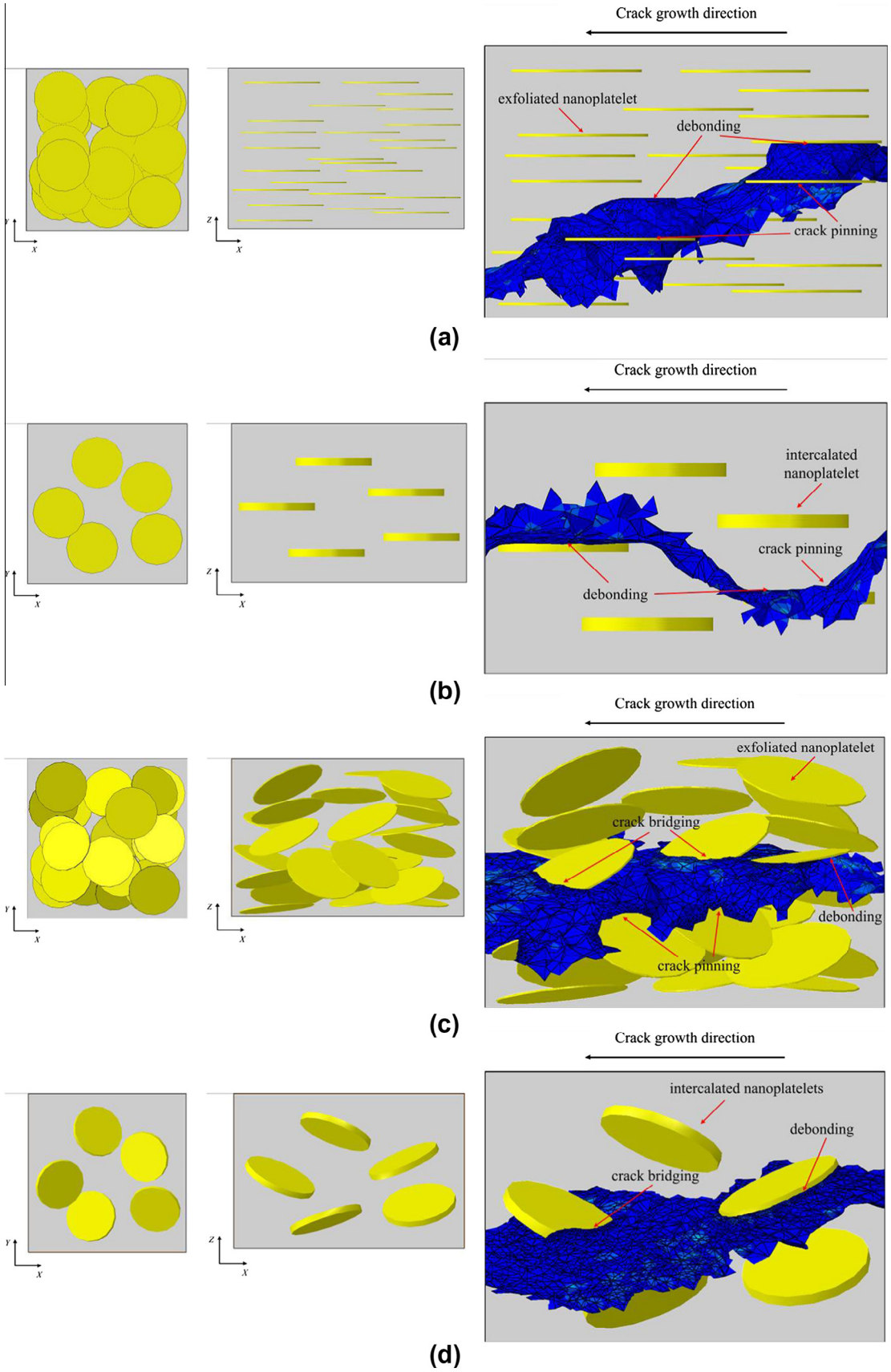

Fig. 3. Submodels located in interface (finer sizing) and the calculated crack path. Left: top and lateral views. Right: crack paths. (a) UCl with 25 aligned exfoliated nanoclays. (b) Aligned cluster reinforced, (c) 25 randomly oriented nanoplatelets (d) 5 randomly distribute clusters.

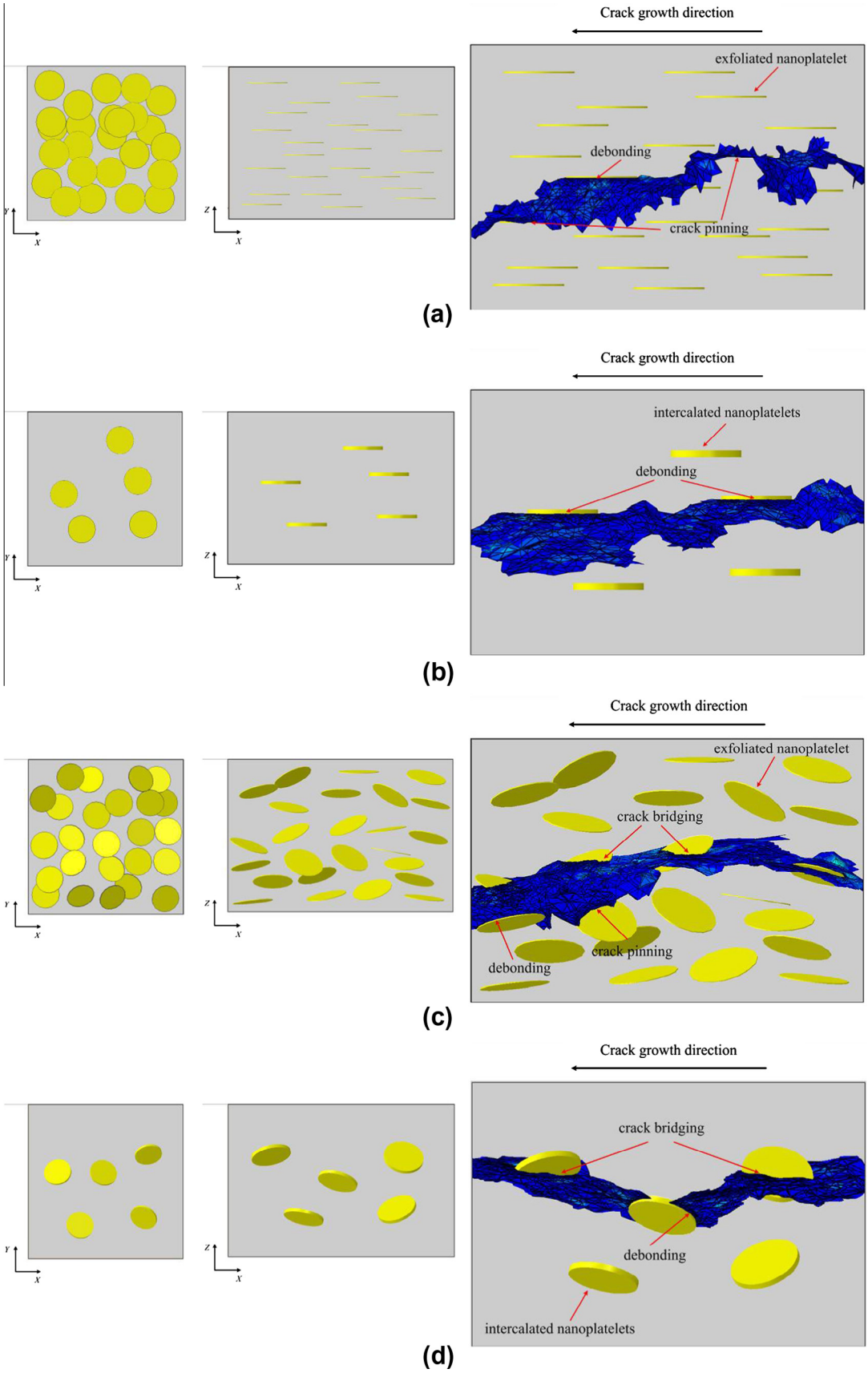

Fig. 4. Submodels located in the matrix and the calculated crack paths. Left: top and lateral views. Right: crack paths. (a) UC with 25 aligned exfoliated nanoclays. (b) Aligned cluster reinforced. (c) 25 Randomly oriented nanoplatelets. (d) 5 Randomly distribute clusters.

nected with each other to form the main crack (again, the similar effects were reported in [4]).

3.2.3. Random exfoliated nanoplatelets reinforcement in matrix

Fig. 4c (left) shows the unit cell model with randomly oriented exfoliated nanoplatelets. All the nanoplatelets are surrounded by the nano-interface layers and distributed and oriented randomly. The angles between the horizontal plane and the nanoplatelet plane were varied in the range 5–50°.

The crack is shown in Fig. 4c (right). The crack bridging, crack pinning and debonding were observed in the crack simulations. The crack path deviation is smaller when compared with Fig. 3c. The crack went through 6 nanoplatelets, with 2 interface debonding and 2 crack pinning cases. In 4 nanoplatelets, crack bridging was observed.

3.2.4. Random intercalated nanoplatelets reinforcement in matrix

Fig. 4d (left) shows the unit cell with random intercalated nanoplatelets reinforcement. All the clusters are distributed randomly. Fig. 4d (right) shows the crack path. The crack went through three clusters. In two places, the crack bridging by platelets was observed. In one place, there was a nanoplatelet–nanoplatelet debonding. This model has the smallest crack deviation when compared with all the above models (except for neat composite).

4. Secondary reinforcements effect on fatigue resistance of multiscale composites

In this section, we seek to compare the observations of the effect of nanoreinforcement on the fatigue fracture mechanisms in the section 3, and to analyze the effect of the secondary reinforcement on the fatigue resistance of composites.

4.1. How secondary reinforcement changes the damage mechanisms

Fig. 5 shows the crack formed near the failed fiber in the composite without secondary nanoreinforcement. The main toughening mechanism in this case is the crack deflection, which is very small when compared to the nanoplatelets reinforced composite results. In the composite with the secondary nanoplatelet reinforcement (whether localized in fiber sizing or in the matrix), various toughening mechanisms are active, among them, crack bridging (Fig. 3b and d, Fig. 4a–d), crack pinning (Fig. 3c and d, Fig. 4a, c and d), interface-nanoplatelets debonding (Fig. 3a, c and d), matrix-nanoplatelets debonding (Fig. 4a, c and d), nanoplatelet-nanoplatelet debonding (3b and d, 4b and d) as well as the crack deflection.

4.2. Crack evolution in different scale level

Here, the global and submodel crack evolution are combined together to present a comprehensive view of the crack development in the fiber and nanoclay reinforced composites. Without the loss of generality, we take the submodels with aligned nanoplatelets reinforcement as examples.

Fig. 6 shows the crack paths in both models considered above (with secondary reinforcement located in the fiber/matrix interface layer, case A, and the nanoplatelets distributed throughout the matrix, case B), macroscale view.

The upper part of each figure shows the cross-section view of a global model, while the lower parts give the crack paths in different regions of the composite.

Comparing the crack paths in the fiber/matrix interface layers, we can see (as expected) that the crack in the interface layer of the case A composite (Fig. 6a) is more rough than that in the case B (nanoreinforcement is distributed over whole matrix, not localized in sizing, Fig. 6b).

Comparing the crack paths in the matrix, one can see that in the case of the matrix without nanoreinforcement (case A) the crack grows straightforward, without deviations, under small angle to the horizontal plane (Fig. 6a). In the case, when the nanoplatelets are distributed in the matrix (case B), the crack changes its direction several times as a result of interaction with nanoplatelets Fig. 6b.

4.3. Studies of the crack deviation parameters

The crack deviation is one of the important mechanisms of the material toughening and the enhancement of the damage resistance. Let us compare the degrees of crack deviation in the considered models. We calculate the parameter of crack deviation, as the maximal *Y*-height of crack path (height of crack peak) minus the *Y*-coordinate of the crack start point (in the submodel unit cell), divided by the *X*-coordinate of the crack peak.

Fig. 7 shows the crack deviation parameters for different nanoplatelets arrangements. One can see that the highest crack deviation parameter is achieved for the aligned exfoliated nanoplatelets arrangements (0.564 if the nanoplatelets are localized in the fiber sizing, and 0.304 if they are distributed throughout the matrix). For the case of the randomly oriented, exfoliated nanoplatelets, the parameter is 0.481 and 0.265, respectively. For the aligned intercalated nanoplatelets arrangement, it is 0.367 and 0.224. The lowest crack deviation is observed in the case of random intercalated nanoplatelets, with 0.314 and 0.205.

If the nanoreinforcement is localized in the fiber sizing, this ensures always larger crack path deviations (due to the higher concentration on nanoplatelets in the volume).

4.4. Fatigue lifetime

In this section, we compare the fatigue resistances of different composites with secondary reinforcement. Fig. 8a presents the *S*–*N* curves obtained for the considered materials.

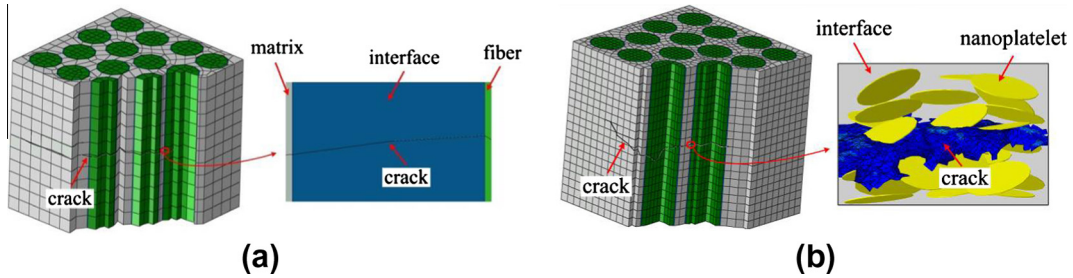

Fig. 5. Crack morphology in fiber reinforced composite with (b)/without (a) secondary nanoplatelets reinforcement.

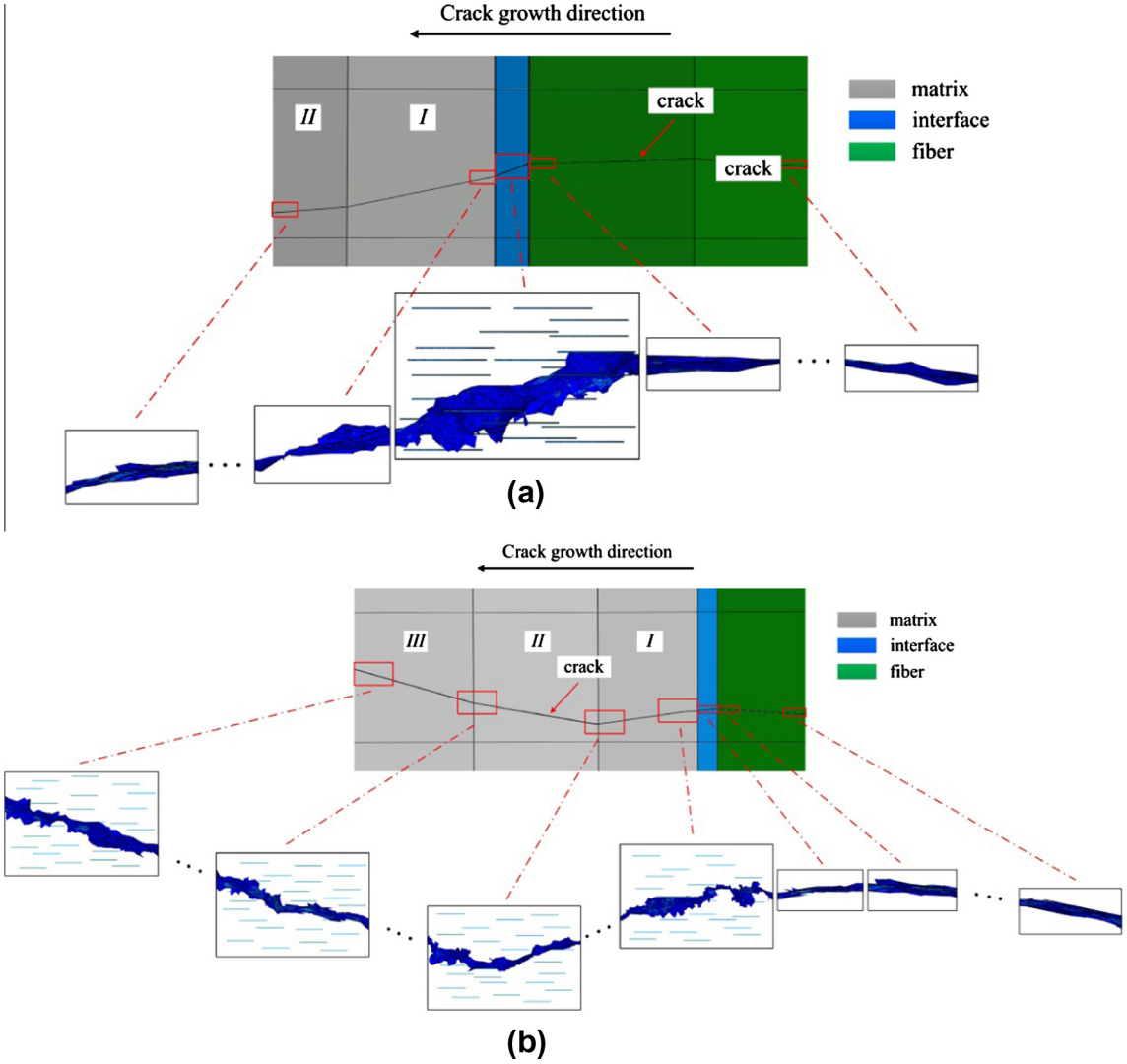

Fig. 6. Crack development in global and submodel (a) in a model with NC in fiber sizing and (b) with NC in a matrix.

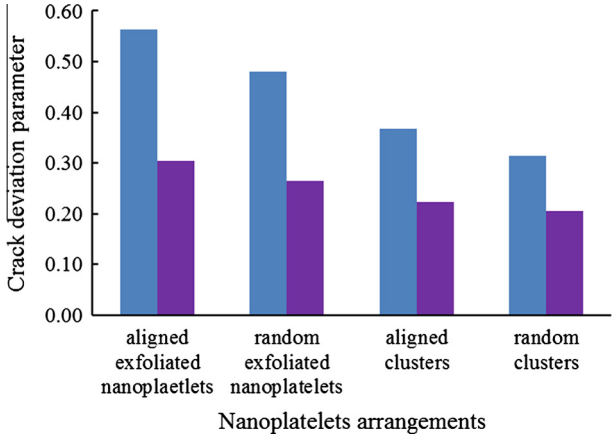

Fig. 7. Crack deviation in different models.

In general, composites with secondary nanoreinforcement show much better lifetime and damage resistance properties than the ones without nanoreinforcement. The composites with nanoreinforcement achieve the same fatigue life (taken exemplarily at 5.68×10^7 cycles) as neat composites, while subject to 2–3.5 times higher loadings. However, this effect is much weaker for the static loading: in the static case, the nanoreinforced composites have only 7–12% higher strength (lower for the composites with nanoplatelets in matrix, higher for the composites with nanoplatelets in the sizing).

Generally, composites with the nanoplatelets localized in the fiber/matrix interface layer (fiber sizing) ensure much higher fatigue lifetime than those with the nanoplatelets in the matrix. Comparing the data on Fig. 8, one can see 43–49% higher applied stress corresponding to the selected lifetime of 5.68×10^7 cycles.

Composites with exfoliated nanoplatelets reinforcement ensure the better fatigue lifetime than those with clustered particles. For instance, for the lifetime 5.68×10^7, the applied compressive loading can be 17–25% (both for nanoreinforcement in sizing and in matrix) higher for nanoreinforced composite with exfoliated structure than for that with clustered structure.

Composites with aligned nanoplatelets or clusters ensure better fatigue resistance than those with randomly arranged clusters. This effect is not fully expected: as observed in Section 3, the randomly oriented nanoplatelets lead to the crack bridging, while aligned platelets promote the crack deviation. Possibly, the controlled, rough crack path influenced by the aligned platelets or clusters has stronger effect on the fatigue life than the crack bridging.

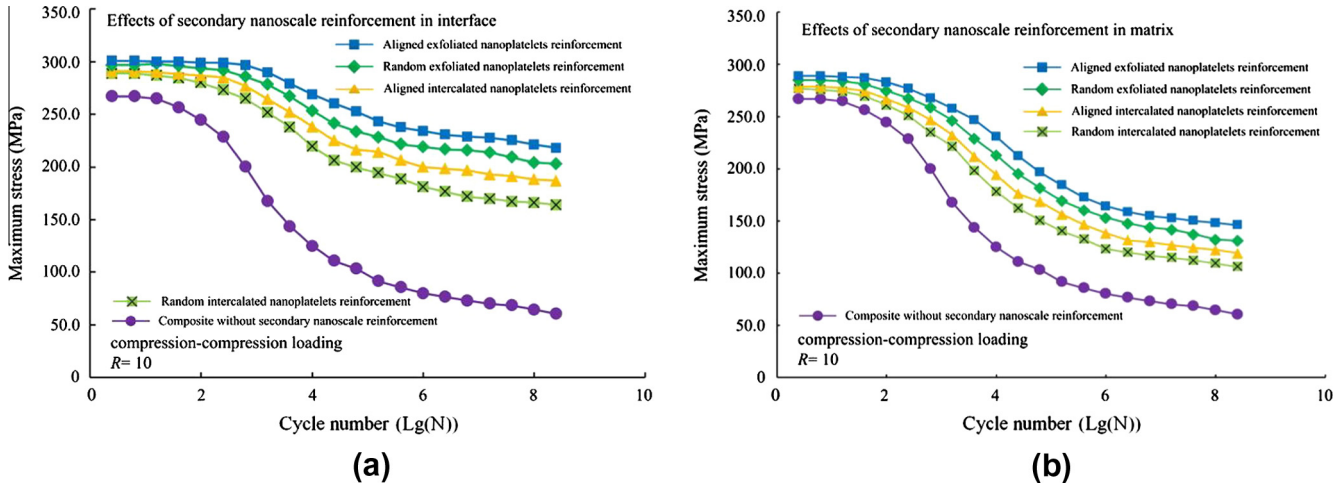

Fig. 8. *S–N* curves for the considered models. (a) Reinforcement in fiber–matrix interface. (b) Reinforcement in matrix.

The fatigue lifetime increases in the following order: neat composite –randomly oriented intercalated nanoplatelets → aligned intercalated → randomly oriented exfoliated → aligned exfoliated. The multiscale composites with aligned exfoliated nanoplatelets in the fiber sizing ensure the highest fatigue lifetime among all the considered structures. Given the correlation with the crack path deviation parameter, one can assume that the fatigue lifetime is strongly controlled by the crack deviation mechanism of toughening.

The positive effect of nanoreinforcement is much stronger when the nanoreinforcement is localized in the fiber sizing. Further, the positive effect of nanoreinforcement is much stronger if (a) the nanoplatelets are aligned, and (b) exfoliated and not clustered.

4.5. Comparison with literature data

It is of interest to compare the data on the effect of the secondary reinforcement on the damage mechanisms and fatigue behavior of the multiscale composites.

Our observation that the availability of nanoclay platelets lead to the repeated crack path deviations and crack changing directions at platelets corresponds to the observations by Xu and Hoa [9], who showed that the fracture surface in fiber composites with epoxy matrix and secondary nanoclay reinforcements is not smooth, but rough, as differed from the nanoreinforcement free, neat material.

The conclusion that the aligned (normally to the fiber axes) high aspect ratio reinforcements ensure better damage resistance than randomly oriented ones can be compared with the results by Qiu et al. [45] and Wicks et al. [46]. While their studies were carried out for secondary carbon nanotube (not nanoclay) reinforcements, they also concluded that aligned, oriented secondary reinforcement ensures the most reliable, high enhancement of damage resistance properties.

Ma et al. [47] studied the effect of nanocomposite coatings on the glass fibers on the properties of composites, and observed the 14.8% increase in strength. In our simulations the nanoreinforcement in sizing lead to the increase in strength by 12%.

Manjunatha et al. [10] reported the strong increase in fatigue life in composites with glass fibers and hybrid particles under WISPERX loading (up to 4–5 times, also a strong increase for the compression-compression and tension–tension loading) as a result of the nanoreinforcement. Evaluating the data from [10] (Figs. 4 and 8), one can estimate that the composite with nanoreinforcement has the amount of same life cycles as the neat composite, when subject to 20–50% higher stress. Khan et al. [8] reported 74% increased fatigue life for 3 wt% clay content in nanoclay/carbon fiber/epoxy composites, however, under tension–tension cyclic loadings. Evaluating the data from [8], one can see that the static strength of the clay-CFRP composites increases to up to 10% due to the nanoclay addition. This is similar to our observations (Section 4.4). Again, the composite with nanoreinforcement can bear around 20% higher load for the same life cycle amount as the neat composite. In our case, the simulations led to the up to 2 times higher compressive load corresponding to the same amount of life cycles. However, since the compressive, matrix controlled properties should be more dependent on the secondary nanoreinforcement, the higher estimations of the composite lifetimes are fully reasonable.

Therefore, the comparison with literature data, even related to different loading conditions and constituents, shows the qualitative resemblance, and confirm the tendencies observed in our simulations.

5. Conclusion

3D multiscale computational models of fiber reinforced composites with secondary nanoscale reinforcements were developed, and used to explore the effect of secondary nanoclay reinforcement, its distribution and geometry, on the fatigue behavior of the composites.

The effect of the nanoclay reinforcement (localized in the fiber/matrix interface (fiber sizing) and distributed throughout the matrix) on the crack path, fatigue damage mechanisms and fatigue behavior is investigated in numerical experiments. Various damage and toughening mechanisms at the nanolevel were observed, among them, crack deflection, crack blocking, bridging, and debonding.

Crack bridging by nanoparticles was observed mainly in composites with randomly oriented nanoplatelets and clusters, while the crack path deviation was strongest in the aligned nanostructures. It was observed that the composites with secondary nanoreinforcement show much better lifetime and damage resistance properties than the ones without nanoreinforcement.

Composites with the nanoplatelets localized in the fiber/matrix interface layer (fiber sizing) ensure much higher fatigue lifetime than those with the nanoplatelets in the matrix.

Composites with exfoliated nanoplatelets reinforcement ensure the better fatigue lifetime than those with clustered particles. Further, composites with aligned nanoplatelets or clusters ensure also higher lifetime than those with randomly oriented nanoreinforcements.

The multiscale composites with aligned exfoliated nanoplatelets in the fiber sizing ensure the highest fatigue lifetime among all the considered structures.

Acknowledgements

The authors gratefully acknowledges the financial support of the Danish Council for Strategic Research (DSF) via the Sino-Danish collaborative project "High reliability of large wind turbines via computational micromechanics based enhancement of materials performances" (Ref. No. 10-094539). Furthermore, the author is grateful to the DSF for its support via the Danish Centre for Composite Structures and Materials for Wind Turbines (DCCSM) (Contract No. 09-067212).

Appendix A. Supplementary material

Supplementary data associated with this article can be found, in the online version, at http://dx.doi.org/10.1016/j.compscitech.2013.11.024.

References

[1] Mishnaevsky Jr L. Micromechanics of hierarchical materials: a brief overview. Rev Adv Mater Sci 2012;30:60–72.
[2] Tang Y, Ye LL, Zhang Z, Friedrich K. Interlaminar fracture toughness and CAI strength of fiber-reinforced composites with nanoparticles – a review. Compos Sci Technol 2013;86:26–37.
[3] Dai GM, Mishnaevsky Jr L. Damage evolution in nanoclay-reinforced polymers: a three-dimensional computational study. Compos Sci Technol 2013;74:67–77.
[4] Siddiqui N et al. Mode I interlaminar fracture behavior and mechanical properties of CFRPs with nanoclay-filled epoxy matrix. Composites A 2007;38:449–60.
[5] Wang HW et al. Nanoreinforced polymer composites: 3D FEM modeling with effective interface concept. Compos Sci Technol 2011;71:980–8.
[6] Rice BP, Chen C, Cloos L, Curliss D. Carbon fiber composites: organoclay–aerospace epoxy nanocomposites. Part I. SAMPE J 2001;37:7–9.
[7] Becker O, Varley RJ, Simon GP. Use of layered silicates to supplementary toughen high performance epoxy carbon fiber composites. J Mater Sci Lett 2003;22:1411–4.
[8] Khan SU et al. Fatigue damage behaviors of carbon fiber reinforced epoxy composites containing nanoclay. Compos Sci Technol 2010;70:2077–85.
[9] Xu Y, Hoa SV. Mechanical properties of carbon fiber reinforced epoxy/clay nanocomposites. Compos Sci Technol 2008;68:854–61.
[10] Manjunatha CM et al. Enhanced fatigue behavior of a glass fiber reinforced hybrid particles modified epoxy nanocomposite under WISPERX spectrum load sequence. Int J Fatigue 2013;54:25–31.
[11] Karippal JJ et al. Study of mechanical properties of epoxy/glass/nanoclay hybrid composites. J Compos Mater 2011;45:1893–9.
[12] Quaresimin M, Varley RJ. Understanding the effect of nanomodifier addition upon the properties of fibre reinforced laminates. Compos Sci Technol 2008;68:718–26.
[13] Pedrazzoli D, Pegoretti A. Silica nanoparticles as coupling agents for polypropylene/glass composites. Compos Sci Technol 2013;76:77–83.
[14] Liu L, Li L, Gao Y, Tang L, Zhang Z. Single carbon fiber fracture embedded in an epoxy matrix modified by nanoparticles. Compos Sci Technol 2013;77:101–9.
[15] Díez-Pascual AM et al. Multiscale fiber-reinforced thermoplastic composites incorporating carbon nanotubes: a review. Current Opinion in Solid State and Materials Science, 2013, http://dx.doi.org/10.1016/j.cossms.2013.06.003.
[16] De Greef N et al. The effect of carbon nanotubes on the damage development of carbon fiber/epoxy composites. Carbon 2011;49:4650–64.
[17] Godara A et al. Interfacial shear strength of a glass fiber/epoxy bonding in composites modified with carbon nanotubes. Compos Sci Technol 2010;70:1346–52.
[18] Godara A et al. Influence of carbon nanotubes reinforcement on the processing and the mechanical behavior of carbon fiber/epoxy composites. Carbon 2009;47:2914–23.
[19] Warrier A et al. The effect of adding carbon nanotubes to glass/epoxy composites in the fibre sizing and/or the matrix. Composites A 2010;41:532–8.
[20] Siddiqui N et al. Tensile strength of glass fibres with carbon nanotube–epoxy nanocomposite coating. Composites A 2009;40:1606–14.
[21] Mishnaevsky Jr L, Brøndsted P. Micromechanical modeling of damage and fracture of unidirectional fiber reinforced composites: a review. Comput Mater Sci 2009;44:1351–9.
[22] Mishnaevsky Jr L. Functionally gradient metal matrix composites: numerical analysis of the microstructure-strength relationships. Compos Sci Technol 2006;66:1873–87.
[23] Qing H, Mishnaevsky Jr L. Unidirectional high fiber content composites: automatic 3D FE model generation and damage simulation. Comput Mater Sci 2009;47:548–55.
[24] Piat R, Schnack E. Hierarchical material modeling of carbon/carbon composites. Carbon 2003;41:2121–9.
[25] Libanori R et al. Hierarchical reinforcement of polyurethane-based composites with inorganic micro- and nanoplatelets. Compos Sci Technol 2012;72:435–45.
[26] Misra RDK, Yuan Q, Chen J, Yang Y. Hierarchical structures and phase nucleation and growth during pressure-induced crystallization of polypropylene containing dispersion of nanoclay. Mater Sci Eng, A 2010;527:2163–81.
[27] Mishnaevsky Jr L, Brøndsted P. Micromechanisms of damage in unidirectional fiber reinforced composites: 3d computational analysis. Compos Sci Technol 2009;69:1036–44.
[28] Mishnaevsky Jr L, Brøndsted P. Three-dimensional numerical modeling of damage initiation in UD fiber-reinforced composites with ductile matrix. Mater Sci Eng A 2008;498:81–6.
[29] Wang HW et al. Single fibre and multifibre unit cell analysis of strength and cracking of unidirectional composites. Comput Mater Sci 2009;46:810–20.
[30] Mishnaevsky Jr L. Micromechanical analysis of nanocomposites using 3D voxel based material model. Compos Sci Technol 2012;72:1167–77.
[31] Krueger R. Development of a benchmark example for delamination fatigue growth prediction. In: Proceedings–american society for composites, 2, no. conf.,2010; 25: 948–967.
[32] Belytschko T, Gracie R, Ventura G. A review of extended/generalized finite element methods for material modeling. Modell Simul Mater Sci Eng 2009;17:1–24.
[33] Mishnaevsky Jr L, Lippmann N, Schmauder S. Computational modeling of crack propagation in real microstructures of steels and virtual testing of artificial materials. Int J Fracture 2003;120:581–600.
[34] Reeder JR. 3D mixed-mode delamination fracture criteria-an experimentalist's perspective. NASA langley research center, M/S 188E, Hampton VA 23681–2199, 2006, USA.
[35] Liao WC, Sun CT. The determination of mode *III* fracture toughness in thick composite laminates. Compos Sci Technol 1996;56:489–99.
[36] Reeder JR. A bilinear failure criterion for mixed-mode delamination. Composite materials: testing and design. ASTM STP 1206, Camponeschi Jr ET, editor. ASTM Int., W. Conshohochen, PA, 1993, pp. 303–322.
[37] Pinho ST, Robinson P, Iannucci L. Fracture toughness of the tensile and compressive fiber failure modes in laminated composites. Compos Sci Technol 2006;66:2069–79.
[38] Jose S, Kuma RK, Jana MK, Rao GV. Intralaminar fracture toughness of cross-ply laminate and its constituent sub-laminates. Compos Sci Technol 2001;61:1115–22.
[39] Krueger R. Development of a benchmark example for delamination fatigue growth prediction. NASA/CR-2010-216723, NIA report No. 2010–04, 2010.
[40] Branco R, Antunes FV, Martins Ferreira JA, Silva JM. Determination of Paris law constants with a reverse engineering technique. Eng Fail Anal 2009;16:631–8.
[41] Seitl S, Kersner Z, Bilek V, Knesl Z. Glass fiber reinforced cement based composite: fatigue and fracture parameters. Appl Comput Mech. 2009;3:363–74.
[42] Creed Jr RF. High cycle tensile fatigue of unidirectional fiberglass composite tested at high frequency. Montana State University; 1993.
[43] Bureau MN, Perrin F, Denault J, Dickson JI. Interlaminar fatigue crack propagation in continuous glass fiber/polypropylene composites. Int J Fatigue 2002;24:99–108.
[44] Fenner JS, Daniel IM. Fracture toughness and fatigue behavior of nanoreinforced carbon/epoxy composites. Experimental mechanics of composite, hybrid, and multifunctional materials, vol. 6. In: Proceedings of the 2013 annual conference on experimental and applied mechanics, springer, 2013.
[45] Qiu JJ, Zhang C, Wang B, Liang R. Carbon nanotube integrated multifunctional multiscale composites. Nanotechnology 2007;18. 275708(11pp).
[46] Wicks SS et al. Model-Experiment Correlation for mode I interlaminar toughening of composite interfaces reinforced with aligned carbon nanotubes. In: ICCM17proceedings, E1.27, July 27–31, Edinburgh, UK, 2009.
[47] Ma PC et al. Development of functional glass fibers with nanocomposite coating: a comparative study. Composites A 2013;44:16–22.